JOURNAL OF SMOOTH MUSCLE RESEARCH

J. Smooth Muscle Res. 2017; 53: 57–72
Published online: June 23, 2017; doi: 10.1540/jsmr.53.57

Review

Role of prostatic interstitial cells in prostate motility

Richard J LANG[1] and Hikaru HASHITANI[2]

[1]*Department of Physiology, School of Biomedical Sciences, Monash University, Clayton Victoria 3800, Australia*
[2]*Department of Cell Physiology, Nagoya City University Graduate School of Medical Sciences, Nagoya 467-8601, Japan*

Submitted March 6, 2017; accepted in final from April 22, 2017

Abstract

The prostate is a gland whose secretions contribute to the seminal fluids ejaculated upon activation of autonomic sympathetic nerves. In elder males, the prostate undergoes an increase in stroma mass and myogenic tone, leading to benign prostatic hyperplasia that occludes the proximal urethra and the presentation of various lower urinary tract symptoms that decrease their quality of life. This review summarises the role of prostatic interstitial cells (PICs) in the generation of the spontaneous tone in the prostate. It presents current knowledge of the role of Ca^{2+} plays in PIC pacemaking, as well as the mechanisms by which this spontaneous activity triggers slow wave generation and stromal contraction. PICs display a small T-type Ca^{2+} current (I_{CaT}) and a large L-type Ca^{2+} current (I_{CaL}). In contrast to other interstitial cells in the urinary and gastrointestinal tracts, spontaneous Ca^{2+} signalling in PICs is uniquely dependent on Ca^{2+} influx through I_{CaL} channels. A model of prostatic pacemaking is presented describing how I_{CaL} can be triggered by an initial membrane depolarization evoked upon the selective opening of Ca^{2+}-activated Cl^- channels by Ca^{2+} flowing only through I_{CaT} channels. The resulting current flow through I_{CaL} results in release of Ca^{2+} from internal stores and the summation of Cl^--selective spontaneous transient depolarizations (STDs) to form pacemaker potentials that propagate passively into the prostatic stroma to evoke regenerative action potentials and excitation-contraction coupling.

Key words: Prostate, prostatic interstitial cells, slow waves, pacemaker potentials, calcium, electrophysiology

Introduction

In the aging male, lower urinary tract symptoms (LUTS) associated with benign prostatic hyperplasia arise from the non-malignant proliferation of the the prostate epithelium and stroma within the transition zone, as well as an increase in the myogenic tone in the encapsulating fibromuscular stroma. Accordingly, current

Corresponding author: Dr RJ Lang, Department of Physiology, School of Biomedical Sciences, Monash University, Clayton 3800, Australia
Phone: +61-3-9905-2517 Fax: +6-13-9905-2547 e-mail: rick.lang@monash.edu

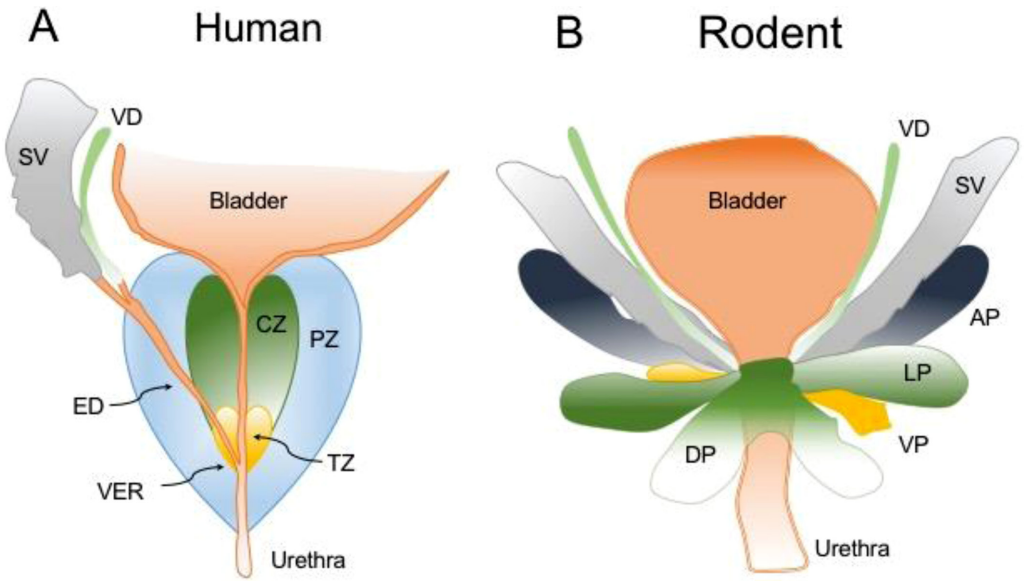

Fig. 1. Schematic comparison of the human (*A*) and rodent (*B*) prostates. Human prostates have been divided into the central zone (CZ) , peripheral zone (PZ) and transitional zone (TZ). In contrast the rodent prostate consists of various lobes radiating from the urethra: AP anterior prostate, DP dorsal prostate, LP lateral prostate and VP ventral prostate. VD vas deferens, SV seminal vesicle, ED ejaculatory duct, Ver vernumontanum.

treatments to effectively relieve the resulting occlusion of the proximal urethra target both the static prostatic enlargement by altering the levels of androgens and estrogens and the dynamic myogenic tone with blockers of α1-adrenoceptors. While the major function of the prostate is to propel its secretions into the seminal fluids upon ejaculation, the prostate in man and rodents also displays spontaneous electrical signals that trigger non-propelling contractile activity. This spontaneous activity possibly serves to move the contents from peripheral prostatic acini towards the prostatic sphincter before ejaculation or maybe prevents stasis and degradation of its contents between ejaculations. This review summarizes current knowledge of the mechanisms by which spontaneous pacemaker activity triggers slow wave generation and excitation-contraction coupling. It also proposes a model of pacemaking that accounts for several major differences to models proposed for spontaneously-active interstitial cells in other urinary and gastrointestinal systems.

Comparing the human and rodent prostate

The prostate in the adult male human is a cone-shaped organ that surrounds the proximal urethra immediately beneath the bladder neck. It is located in the pelvic cavity posterior to the symphysis pubis and anterior to the bladder and rectum. The base of the prostate cone lies immediately under the bladder neck, while its apex faces downwards abutting the urogenital diaphragm and the striated sphincter. The ejaculatory ducts which are formed by the junction of ampullae of the vas deferens and seminal vesicles enter at the base of the prostate and pass obliquely through to join the prostatic urethra at the vernumontanum (Ver Fig. 1A). The human prostate has also been described as consisting of several regions. The anterior fibromuscular stroma containing mostly smooth muscle fibres extends from the bladder neck to the striated sphincter. The central zone (CZ) a wedge shaped glandular region with its base at the bladder neck surrounding the ejaculatory ducts, while its apex ends at the vernumontanum (Fig. 1A) (1). The peripheral zone (PZ) is a funnel shaped glandular region surrounding the central zone and the urethra beyond the vernumontanum (Fig. 1A) and represents the area mostly

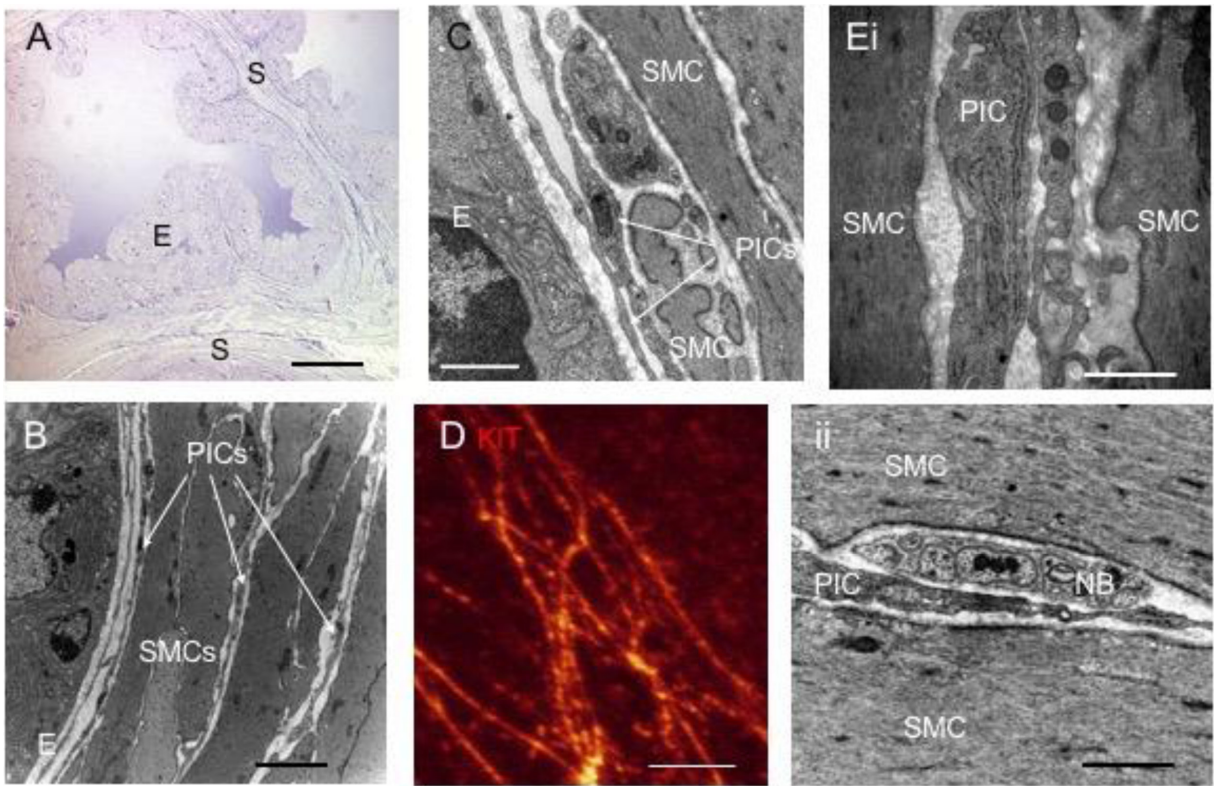

Fig. 2. PICs in the guinea pig prostate. *A, B* acini in the ventral lobe consists of a lumen surrounded by glandular secretory cells enveloped by a stroma of PICS and SMCs. PICS are located between the epithelial and stromal layer (*B*, *C*) and within and between the SMCs (*B*). *D* Kit immune-reactivity in the guinea-pig prostate. *Ei* higher magnification reveals PIC internal organelles such as rough endoplasmic reticulum and caveolae. *Eii* Nerve bundles form close associations with both SMCs and PICs within the stroma. Scale bars represent A 50 µm; B 2 µm; C, Eii 1 µm; D 2 µm; Ei 0.5 µm. Figure adapted from Exintaris et al., (2002) (5) and Hashitani & Lang (2010) (44).

susceptible to adenocarcinoma and prostatitis. Finally, the preprostatic region consists of prostatic sphincter, the periurethral glands and the inner transitional zone (TZ), the region in which benign prostatic hyperplasia mostly originates (2).

In rodents such as the mouse and guinea pig, the prostate consists of a number of lobes located circumferentially around the urethra, with their peripheral ends extending into the pelvic cavity (Fig. 1B). Anterior to the urethra, the ventral prostate (VP) partially wraps around the urethra. The VP is flanked by two lobes of the lateral prostate (LP), while the dorsal prostate (DP) forms a butterfly shape structure at the base of the seminal vesicles (Fig. 1B) (2). Based on their mRNA expression the mouse anterior prostate (AP), sometimes called the coagulating glands, is thought to be the counterpart of the human prostatic CZ, while the dorsal lateral prostatic (DP and LP) lobes are thought to resemble the PZ (2, 3). Even though there is no equivalent area to the human TZ, the guinea pig prostate displays considerable hypertrophy with age (>30 months) associated with an increased stromal mass and a significant stromal fibrosis (4).

Prostatic interstitial cells (PICs)

Electron microscopic investigations of the stroma surrounding the acini within the peripheral lobes of the guinea pig (Fig. 2A) (5) and gerbil (6) prostate have established that numerous interstitial cells lay within the sub-urothelial space between the epithelium and muscle layer, and between and within the muscle bundles (Fig. 2B, C). These prostatic interstitial cells (PICs) display many of the established internal structures, such

as an extensive smooth endoplasmic reticulum (Fig. 2C, Ei), bundles of intermediate filaments, large Golgi apparatus, numerous caveolae and mitochondria, a discontinuous basal lamina (Fig. 2Ei) and close associations with neighbouring nerve bundles (Fig. 2Eii) (5, 6), that define the presence of interstitial cells of Cajal (ICC), the pacemaker cells in the gastrointestinal tract.

Kit-positive PICs

As with gastrointestinal ICC, PICs in the prostate of mouse (7), human (8, 9), rat (10) and guinea pig (Fig. 2D) (5, 11) are labelled by antibodies raised against the Kit receptor (CD117) of the receptor tyrosine kinase. These Kit-positive PICs are either spindle or stellate shaped, lying in the same morphological spaces identified under the electron microscope, within the stroma between the muscle and the epithelial layers, and within or parallel to the long axis of α-smooth muscle actin-positive muscle bundles (5, 10, 12). Kit-positive PICs also run parallel to and form close appositions with tyrosine hydroxylase-positive, dopamine β-hydroxylase-positive sympathetic nerve bundles. Double labelling also reveals that Kit-positive PICs co-locate with immuno-reactivity indicating the presence of the gap junction protein, connexion 43 (CX43). PICs also display a stronger immuno-reactivity for α_1-adrenoceptor protein than neighbouring SMCs (12). However, Kit-positive PICs may well represent only a subpopulation of the interstitial cells present, as Kit-negative vimentin-positive cells have also been reported, particularly in the sub-urothelial space of the guinea pig prostate (13).

In W/W^v mice, in which the GI tract distribution of Kit-positive ICC is severely but not evenly disrupted, the prostate is transiently smaller between 4 and 8 weeks of age. Kit antibodies also reduce the size and the number of branching points of 4-day old wildtype prostates placed in organ culture for a further 4 days (7). These cultured prostates have an increase basal/ luminal cell ratio but do not have any apparent defects in their stromal cell recruitment, their vasculature or survival of the prostate epithelium (7). Kit signalling has been implicated in cell proliferation associated with benign prostatic hyperplasia (14) and cancer development (15). However, Kit-positive PIC numbers are not significantly altered in patients with diabetes (16). Combined treatment of an aromatase inhibitor and an anti-androgen agent results in a general atrophy of the dog prostatic acini that is less severe than castration (17), while oestrogen-treated rats displayed a significant reduction in prostatic weights associated with an increased number of Kit-positive PICs (10). A subpopulation of Kit-positive stem cells in the mouse prostate can also be induced to generate a prostate after transplantation (7).

Electrophysiology of the prostate

Slow waves

Spontaneous contractile activity has been demonstrated in strips of prostatic stroma of guinea pig (5, 18), rabbit (19) and human (20, 21). Impalements of SMCs within the guinea-pig prostatic stroma with intracellular microelectrodes reveals the presence of spontaneous slow waves that consist of a slowly rising depolarizing transient that triggers a number of large amplitude action potentials and stromal contraction (Fig. 3Bi-ii). The depolarizing transients can be quite variable in amplitude, being either > 10 mV (22) or being barely visible (11) before the action potential discharge (Fig. 3Bi-ii). The rapid repolarization of the action potential is followed by a short plateau (5, 22). Upon addition of an 'L-type' voltage dependent Ca^{2+} channel (LVDCC) blocker (1 μM nifedipine), the action potentials are abolished and the slow wave duration and muscle contraction reduced, so that the underlying depolarizing transient is often larger and shorter due to the the reduction of any outward or inward membrane conductances activated of upon LVDCC Ca^{2+} entry (5, 13, 23). On the occasions that the depolarizing transients are very small, 1μM nifedipine appears to completely block slow wave discharge. It

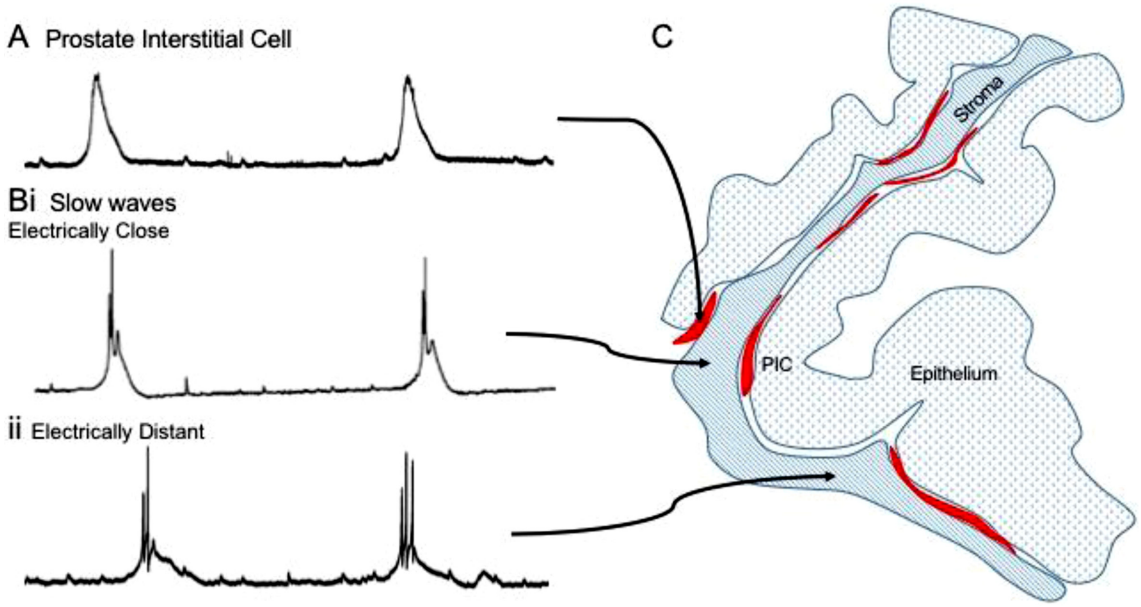

Fig. 3. Typical recordings of pacemaker potentials (*A*) and slow waves electrically close (*Bi*) and distant (*Bii*) from the intracellular recording electrode. *C* schematic of arrangement of PICs and SMC stroma with respect to the recordings in *A, B*. Traces adapted from Lang et al. (2006) (22).

seems likely that the varying amplitude of the depolarizing transients reflexes the passive decay with distance between their site of generation and the recording electrode, while their active propagation is dependent on the regenerative activation of LVDCCs in individual stromal SMCs (Fig. 3Bi-ii) (22). The frequency of the depolarizing transients are little affected by 1–10 μM nifedipine (5, 13).

Removal of Ca^{2+} from the bathing solution completely blocks all electrical and contractile activity (5) confirming the fundamental role of Ca^{2+} entry in the generation of slow waves and stromal wall contraction. A voltage dependence of this Ca^{2+} entry and slow wave generation is evident when directly shifting the stromal membrane potential with external K^+ concentration manipulations, current injection (13), K_{ATP} channel openers (13) or blockers of voltage-dependent K^+ channels (23), to either more hyperpolarized or depolarized levels which decreases or increases, respectively, the frequency of slow wave firing. Depolarizing transients recorded in the presence of higher concentrations of nifedipine (3 and 10 μM), are further reduced upon the addition of a 'T-type' voltage-dependent Ca^{2+} channel (TVDCC) blocker (10 and 100 μM Ni^{2+} or 1 μM mibefradil) (13). Any residual spontaneous contractions in nifedipine are also abolished upon this blockade of both TVDCCs and LVDCCs (13).

Pacemaker potentials

Occasionally, recordings are made from cells in the guinea pig prostate that display electrical events consisting of a large depolarizing phase which triggers a small repolarization, a very long plateau and a slow decay phase (Fig. 3A) (22). The plateau phase of these pacemaker potentials is reduced considerably in the presence of nifedipine (13). The resting membrane potential and frequency of discharge (5–6 min^{-1}) of these pacemaker cells is not significantly different from the same parameters of cells displaying slow waves (5, 13, 22, 24).

Spontaneous transient depolarizations (STDs)

Many preparations of the guinea pig prostate display STDs in the absence or presence of slow wave firing (22) and in the absence or presence of LVDCC blockers (25). Probability density analysis of STD parameters suggests that they can be divided into two populations: larger rapidly-rising STDs and smaller STDs with slower time courses (22), leading to the initial speculation that these two populations of STDs reflect injections of depolarizing current into the stromal syncytium that are electrically close and distant, respectively, from the recording electrode (22). STDs also fire in clusters or bursts, rather than randomly, evident by the often-observed summation of STDs (22) which form membrane depolarizations similar in time course as pacemaker potentials but which don't elicit a slow wave or stromal contraction (13).

Electrical propagation in the prostatic stroma

Twin intracellular microelectrode recordings in lobes of the guinea pig prostate have confirmed that slow waves in the absence or presence of nifedipine propagate between cells, while STDs fail to do so (25). This propagation of slow waves and associated stromal contraction can be rapidly and reversibly abolished using gap junction uncouplers (18β-glycyrrhentinic acid, carboxolone or octanol) (26). Pacemaker potentials, slow waves and STDs are also all abolished in a concentration dependent manner by blockers of Ca^{2+}-activated chloride channels (CaCCs), niflumic acid (NFA), flufenamic acid and anthracene-9-carboxylic acid (9-AC), but not by 4.4'-diisothiocyanostilbene-2,2' disulphonic acids (DIDS) (22, 24).

Given that rodent prostatic lobes consist of numerous epithelium-lined acini surrounded by a stroma containing a single layer of PICS enveloped by a SMC layer a few cells thick (Fig. 2A), it is likely that most intracellular recordings are made from the SMC layer which presumably exists as an electrical syncytium, albeit of a very complex arrangement (Figs. 2A-B, 3C) (5, 11). It is likely that PIC pacemaker potentials are generated upon the summation of a number of simultaneously-occurring STDs, while the depolarizing transient of individual slow waves represents the passively-propagated membrane response of a pacemaker potential generated in neighbouring PICs. The varying amplitude and time course of STDs and depolarizing transients merely reflexes the varying distance between the site of their generation in the stromal syncytium and the recording electrode (Fig. 3A, Bi-ii) (22). Ca^{2+} entry through LVDCCs appears responsible for the generation of the plateau of the pacemaker potential and slow wave, while Ca^{2+} entry through TVDCCs contributes to their rising phase, both presumably activated upon the opening of CaCCs. STDs, being recorded in the presence of blockers of both LVDCCs and TVDCCs and blocked by niflumic acid or Ca^{2+} free solutions, suggest that they are CaCC currents generated by mechanisms of Ca^{2+} mobilization from internal stores.

Stromal action potentials

Large, brief, nifedipine-sensitive action potentials are readily triggered by the slow-wave depolarizing transient. In both pubescent (400 g) and mature (>1 kg) guinea pig prostates, spontaneous action potentials are sometimes recorded, often at high frequencies in cells that do not display slow wave activity (27). STD amplitudes in these cells appear to be sufficiently large to directly trigger action potential firing without their need to sum into a pacemaker potential. In mature prostates, very high frequency nifedipine-sensitive action potential discharged can also be recorded in 'hyperactive' cells (27). It appears that the membrane potential of these regions of the stromal syncytium is intrinsically close to the threshold of action potential discharge so that the SMCs themselves are directly generating the spontaneous electrical and contractile activity. This electrical behaviour resembles action potential activity in strips of guinea pig bladder (28) and perhaps reflects an aged-induced collapse of the stromal syncytium into independent regions of iso-potential 'short cables'.

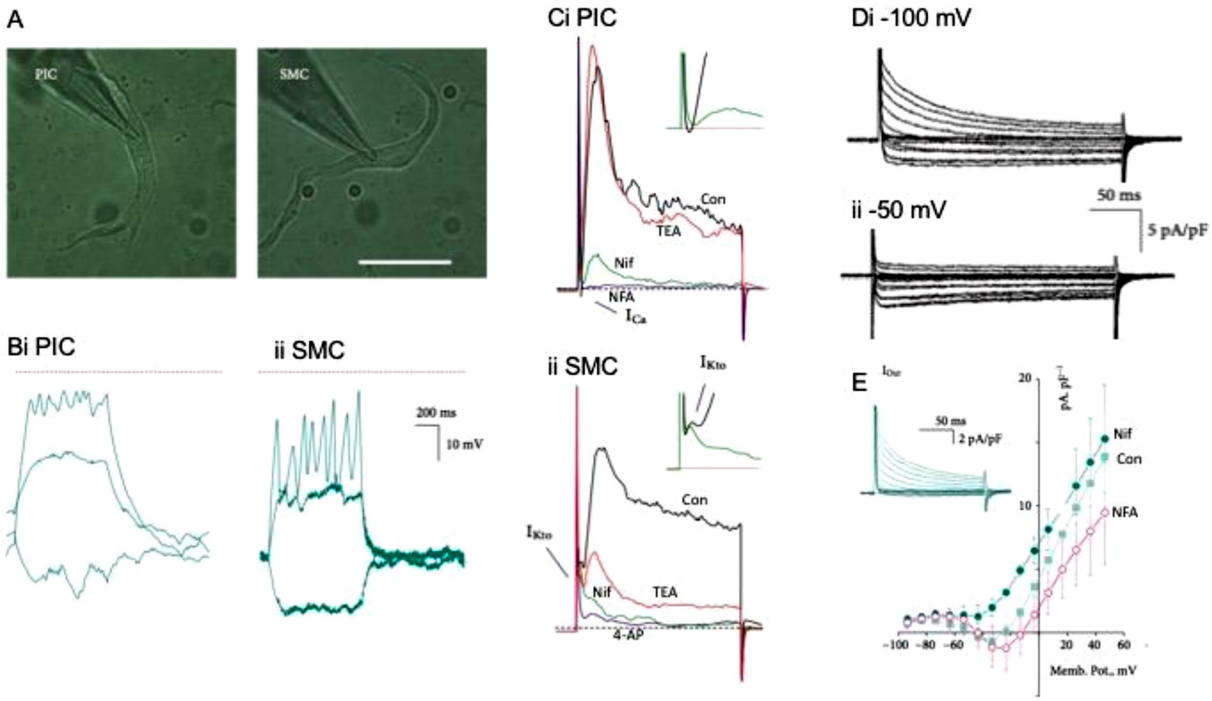

Fig. 4. Comparison of the ultrastructure and electrical activity in freshly isolated PICs and SMCs of the guinea-pig prostate. PICs are readily identified by their spikey appearance (*A*), by the absence of action potential firing under current clamp (*Bi*) and their differing ion channel expression, notably the absence of I_{Kto} and the presence of a substantial niflumic acid-sensitive CaCC (*Ci-ii*). PICs express a niflumic-acid-sensitive outward current (*E*) that is blocked by conditioning voltage steps that would selectively inactivate I_{CaT} and not I_{CaL} (*Di-ii*). Con control; Nif nifedipine, NFA niflumic acid. Figure adapted from Lang et al. (2014) (32).

This creation of multiple short syncytia generating continuous tone within the mature prostate may well be a consequence of the increase stromal fibrosis with age (4).

PIC and SMC ion channel currents

Single human (29, 30) and guinea-pig (Fig. 4Bii) (31, 32) prostatic SMCs can generate large brief action potentials upon electrical depolarization (Fig. 4Bii). Under voltage clamp, these SMCs display a large nifedipine- and verapamil-sensitive LVDCC current (I_{CaL}) with a voltage of half-maximal activation near –20 mV in the guinea pig (31) and –7 mV in the human (30). Human prostatic SMCs also express a Ni^{2+}-sensitive TVDCC current (I_{CaT}) with a half maximal activation of –36 mV and a half maximal inactivation (availability) of –53 mV (30). Both human and guinea-pig prostatic SMCs display a 'window current' between –60 and 0 mV (30, 31), suggesting the presence of a slowly-inactivating, near constant Ca^{2+} entry within this membrane potential range. The amplitude of I_{Ca} in human prostatic SMCs is increased in a concentration dependent manner by phenylephrine, which is prevented upon blockade of both pertussis toxin-sensitive and –insensitive G proteins. The increase in I_{Ca} and resulting rise in internal Ca^{2+} concentration ($[Ca^{2+}]_i$) in these single SMCs upon α1-adrenoceptor stimulation is mimicked by intracellular-applied inositol trisphosphate (IP_3) and attenuated by ryanodine, thapsigargin or intracellular heparin. Cyclic nucleotides cAMP and cGMP have little affect on I_{Ca} or $[Ca^{2+}]_i$ (29). These data suggest that the release of Ca^{2+} from both ryanodine receptor (RyR)-dependent and IP_3-depedent Ca^{2+} stores are involved in this α1-adrenoceptor stimulated rise in $[Ca^{2+}]_i$, while increased levels of Ca^{2+} / diacylglycerol levels may well be stimulating protein kinase C to increase I_{Ca} (29).

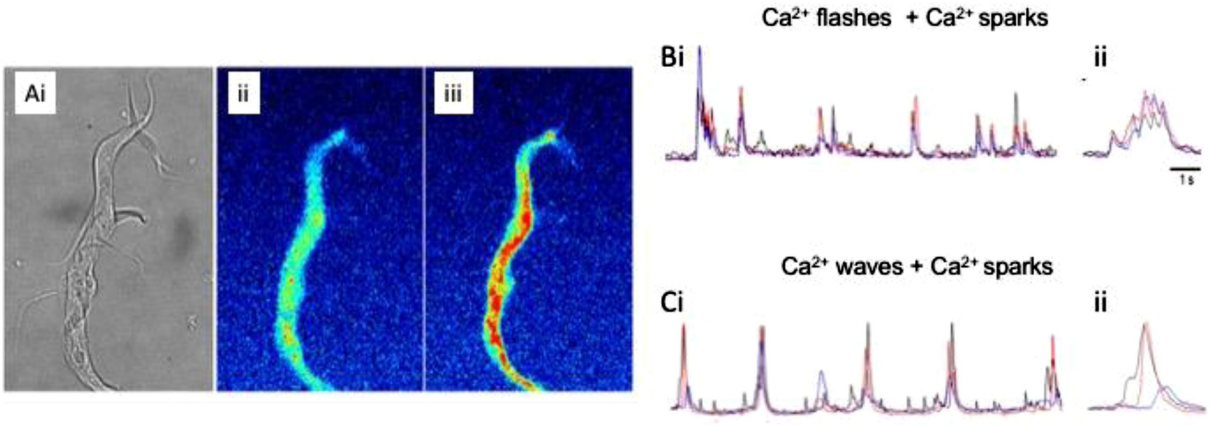

Fig. 5. Ca^{2+} signals in PICs. Single PICs under bright field (*Ai*) and fluo-4 fluorescence illustrating a rise in $[Ca^{2+}]_i$ (red) upon exposure to a high K^+ solution without cell shortening (*Aii-iii*). Ca^{2+} flashes (*Bi*) and Ca^{2+} waves (*Ci*) displayed on expanded time scale (*Bii, Cii*) illustrating their differing time course and synchronicity. Figure adapted from Lam et al. (2011) (40).

Membrane depolarization of guinea-pig SMCs under voltage clamp also triggers a rapidly-rising 4-aminopyridine (4-AP)-sensitive transient K^+ current (I_{Kto} Fig. 4Cii) with voltages of half-maximal activation (near 0 mV) and half-maximal inactivation (near –60 mV) (31, 33) that suggest 2.5% of these channels would be contributing to the resting membrane potential, and that only 40% of these channels would be available for opening upon further membrane depolarization (31).

In guinea pig (Fig. 4Cii) (31–33) and human (30) prostatic SMCs, membrane depolarization also triggers a second slowly-rising outward current which slowly decays over 100s of milliseconds. This outward current is readily blocked by tetraethylammonium (TEA) (31–33) at concentrations that selectively block large conductance Ca^{2+}-activated K^+ (BK) channels, or when impermeant Cs^+ replaces K^+ in the recording pipette (30). Whole-cell BK currents are irreversibly inhibited by CPA or ryanodine supporting the notion that these channels are activated by the Ca^{2+}-induced Ca^{2+} release (CICR) from ryanodine-sensitive Ca^{2+} stores. Spontaneous transient outward currents (STOCs) arising from the bursting activation of a number of BK channels upon the spontaneous release of stored Ca^{2+} are also inhibited by another BK blocker, iberiotoxin, and transiently accelerated and then blocked by 10 mM caffeine which is thought to open RyR channels and rapidly deplete the Ca^{2+} store (33). Single channel analysis of the BK channels in guinea-pig SMCs reveals that they have a single channel conductance of 270 pS and are activated by both voltage and $[Ca^{2+}]_i$. Their voltage of half- maximal activation shifts significantly in the negative direction as $[Ca^{2+}]_i$ is raised (between 15 and 1540 nM), their Ca^{2+}concentration of half-maximal activation is 625 nM (31).

PIC currents

In addition to their ‘spikey morphology (Fig. 5Ai), single PICs isolated from the guinea prostate are distinguished from SMCs by their inability to evoke an action potential (Fig. 4Bi), the absence of an I_{Kto}, and the presence of a large nifedipine-sensitive I_{CaL} (Fig. 4Ci, Dii) and a large TEA-resistant, Cl^--selective outward current that is reduced by niflumic acid (Fig. 4Ci, Di, E) (32). 50% of PICs also express a very small Ni^{2+}-sensitive I_{CaT}. The large Cl^--selective current is blocked by membrane depolarization that selectively blocks I_{CaT}, but leaves I_{CaL} intact (Fig. 4Di-ii), or when Ca^{2+} is replaced by Ba^{2+} (32). Thus, 50% of PICs express an Cl^- current current that is selectively activated by Ca^{2+} that flows only through PIC TVDCCs and not LVDCCs. Its is likely that these TVDCCs and CaCCs are in close apposition within in a confined sub-membrane compartment of the

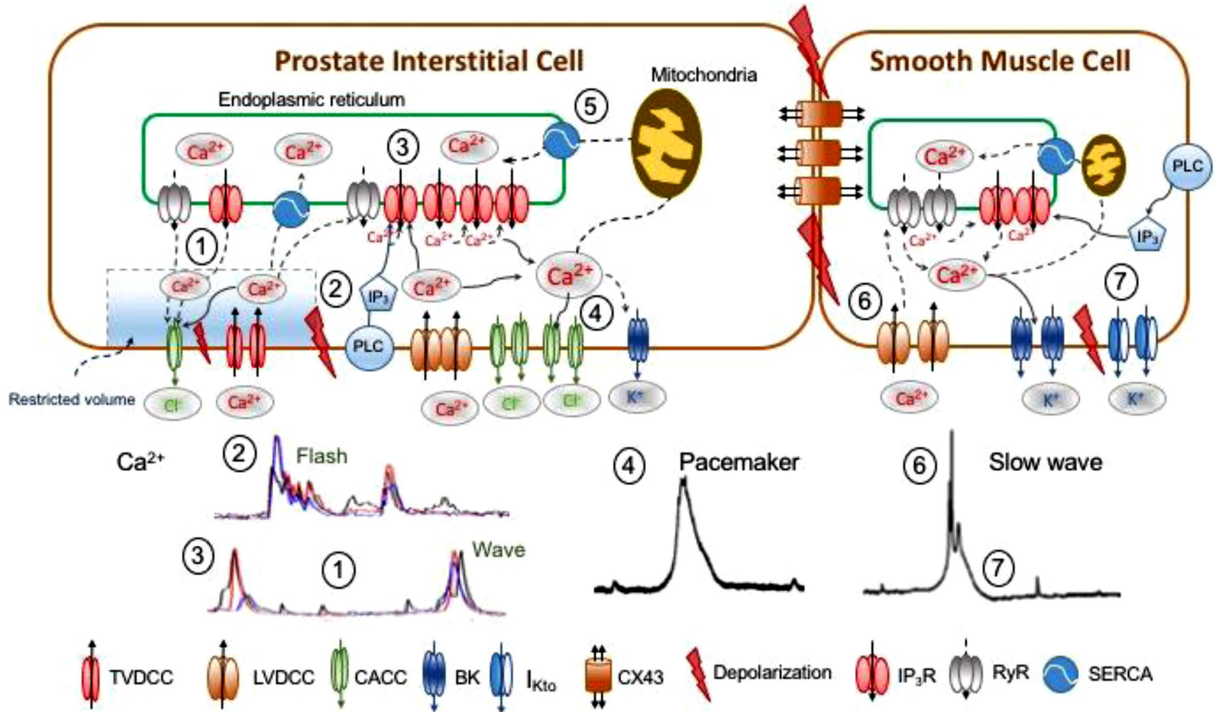

Fig. 6. Model of the role of Ca^{2+} in PIC pacemaking in the guinea pig prostate. This model incorporates current knowledge of the ion channel expression and Ca^{2+} signals in PICs and SMCs. *1* initial release of Ca^{2+} and opening of TVDCCs and activation of CaCCs within a restricted sub-membrane space; *2* depolarization activation of PLC or LVDCCs; *3* CICR of IP_3R and RyRs; *4* STD summation into a pacemaker potential; *5* Ca^{2+} levels returned to control via SERCA pump and mitochondrial buffering; *6* pacemaker potential propagates into SMCs triggering LDCC action potentials.; *7* action potential repolarization involving voltage dependent I_{Kto} and CICR from RyR stores to activate BK channels. See text for details.

PIC (Fig. 6). Large inward currents are also evoked in single guinea-pig PICs in culture upon α1-adrenoceptor stimulation with norepinephrine (1–100 μM) in a manner prevented by phentolamine or prazosin (12).

As the plateau duration of the pacemaker potential is reduced considerably upon I_{CaL} blockade (13), Ca^{2+} entry through LVDCCs outside of the restricted compartment must also be activating additional CaCCs (Fig. 6). By analogy with the role of intramuscular ICC (ICC-IM) generating the second component of the slow waves in the gastrointestinal tract (34), these LDCCs could also be in neighbouring PICS that don't express I_{CaT}.

Effects of K^+ channel blockers on slow waves

Being a syncytium it is difficult to attribute the effects of various K^+ channel blockers on whole-tissue preparations to a specific action on PICs or stromal SMCs, or both. BK channel blockers, TEA and iberiotoxin and the I_{Kto} blocker 4-AP all increase slow wave frequency, while a blocker (apamin) of small-conductance Ca^{2+} activated (SK) channels has little effect (23). Direct (levcromakalim, Y-26763 or PCO-400) and indirect (sodium nitroprusside (SNP) or calcitonin gene-related peptide (CGRP)) activators of K_{ATP} channels hyperpolarize the stromal syncytium and block slow wave firing in a manner reversed by the K_{ATP} channel blocker glibenclamide (13, 23). Given that stromal SMCs selectively express I_{Kto} and appear to have a greater expression of BK channels than PICs (32), their blockers are presumably affecting the ability of the stromal syncytium to receive and propagate the pacemaker drive by reducing an intrinsic 'refractory' (BK) membrane conductance between individual slow waves. Subthreshold STDs are still evident during the opening of K_{ATP} channels as the syncytium's membrane potential is maintained negative of the threshold of pacemaker and slow wave generation (13, 23).

Role of internal Ca^{2+} stores

Blockade of Ca^{2+} uptake into internal stores via the sarco-endoplasmic reticulum Ca^{2+}ATPase (SERCA) pump with cyclopiazonic acid (CPA) results in a transient acceleration of slow wave activity followed by a sustained membrane depolarization (4–10 mV) and a gradual reduction or abolition of STD and slow wave activity over 20 min (11, 24). A similar inhibition and membrane depolarization occurs upon the blockade of mitochondria buffering of cytosolic Ca^{2+} with cyanide m-chlorphenyl hydrazine (CCCP) (22), p-trifluoromethoxy carbonyl cyanide phenyl hydrazine (FCCP) or the respiratory chain inhibitor, rotenone (24, 35).

The frequency of pacemaker potentials and slow wave firing and their associated contractions are initiated (18) or accelerated by G-protein coupled receptor agonists (noradrenaline, phenylephprine, histamine or carbachol) that stimulate phospholipase C (PLC) metabolism of phosphatidylinositol 4,5-bisphosphate (PIP_2) to inositol trisphosphate (IP_3). IP_3 evokes the release of stored Ca^{2+} via IP_3 receptor (IP_3R)-gated channels, in the absence or presence of nifedipine (5, 11, 35). Conversely, stroma contractions and slow wave frequencies are reduced when IP_3-dependent Ca^{2+} release is inhibited with 2-aminoethoxy-diphenylborate (2-APB), when phospholipase C formation of IP_3 is blocked with U73122 or neomycin, or when IP_3 binding is antagonised with xestospongin C (24).

In contrast, the sustained opening of RyR channels and depletion of their stores with ryanodine only produces a small transient acceleration of slow wave firing, so that slow wave frequency is little different from control after 30 min exposure (24). Caffeine (1 mM) also reduces the frequency of slow wave frequency associated with little changes in their time course and a significant membrane depolarization (22, 24). However, this exposure of the guinea pig prostate to 1 mM caffeine appears to be too low a concentration to be confident it is acting solely on RyRs. Instead, caffeine (at 1 mM) has been suggested to be acting on IP_3R Ca^{2+} release channels (36) or increasing levels of cGMP upon inhibition of cytosolic phosphodiesterases (37).

Ca^{2+} signals in PICs

To date, there has only been one report describing the spontaneous Ca^{2+} signals in the guinea pig stroma and freshly-isolated PICs (Fig. 5A) (25). Whole mount prostatic preparations display Ca^{2+} flashes that occur simultaneously along the full length of individual SMCs and near synchronously in all cells within the field of view, resulting in stromal wall contraction. Individual SMCs within the syncytium also display slowly-moving Ca^{2+} waves along their longitudinal axis.

In contrast, freshly-isolated PICs display three spontaneous Ca^{2+} signals: whole-cell Ca^{2+} flashes (Fig. 5Bi), slowly-propagating Ca^{2+} waves (Fig. 5Ci) and localized Ca^{2+} sparks (Fig. 5Bi, Ci) (25). Ca^{2+} flashes and Ca^{2+} waves are readily distinguished by their differing latencies between transients when recordings are made from 2–3 different regions within individual PICs (Fig. 5Bii, Cii), while Ca^{2+} sparks do not propagate within cells. Ca^{2+} flashes are significantly smaller in amplitude than Ca^{2+} waves and occur in bursts, at a frequency twice that of Ca^{2+} waves (25). Ca^{2+} flashes and Ca^{2+} waves are blocked by nominally Ca^{2+}-free solutions and upon Ca^{2+} store depletion with 10 μM CPA or 10 mM caffeine (25) suggesting that the generation of spontaneous Ca^{2+} signals is intimately dependent on Ca^{2+} entry and the release of Ca^{2+} from internal RyR-sensitive Ca^{2+} stores.

In contrast to Ca^{2+} signals in whole mount prostatic preparations, Ca^{2+} flashes and Ca^{2+} waves in single PICs are completely blocked by another LVDDCC blocker,1 μM nicardipine (25). It is not yet clear whether the incomplete block in the whole mounts preparations reflects an access barrier for dihydropyridine LVDDCC blockers. Such an incomplete block would explain the continued presence of pacemaker potentials and depo-

larizing transients in 1 μM nifedipine (5, 22). Alternatively, the complete blockade of Ca^{2+} signals in single PICs can be explained if the fluorescent Ca^{2+} indicator used did not have access to the restricted sub-membrane space occupied by TVDCCs responsible for the initial activation of CaCCs (32).

Model of PIC pacemaking

Figure 6 summarizes current knowledge of the ion channel compliment and Ca^{2+} signalling mechanisms underlying the generation of the PIC pacemaker potential. The initial event of rhythmicity is likely to be the generation of small STD arising from the opening of a few CaCCs by a Ca^{2+} 'spark' or 'puff' upon the spontaneous release of Ca^{2+} from RyR- or IP_3R-gated channels (*1* in Fig. 6), possibly primed by rising Ca^{2+} levels in the internal stores sensitizing the Ca^{2+} release channels (38). The resulting membrane depolarization triggers the opening of Ni^{2+}-sensitive TVDCCs, the Ca^{2+} that enters through these channels then activates more CaCCs within a restricted sub-membrane space to create a larger detectable STD. These STDs could be large enough to trigger further Ca^{2+} entry upon the opening of LVDCCs (Ca^{2+} flashes). Alternatively, STD summation may further facilitate CICR possibly via a voltage-dependent PLC production of IP_3 (*2* in Fig. 6). The resulting rise in $[Ca]_i$ sequentially activates the Ca^{2+} store-TVDCC complexes upon the activation of RyRs and IP_3Rs in neighbouring compartments to develop Ca^{2+} waves involving Ca^{2+} entry through LVDCCs (*3* in Fig. 6). This entrainment/ amplification by Ca^{2+} entry through LVDCCs to create larger and more frequent STDs may also provide an alternate explanation for the presence of 2 populations of STDs described in Lang et al. (2006). Summation in time of individual STDs generates the pacemaker potential (*4* in Fig. 6). The termination of CaCC activation upon cessation of Ca^{2+} release due to reduced luminal Ca^{2+} determines the duration of the plateau phase of the pacemaker potential (38). Ca^{2+} levels are returned to resting levels between pacemaker potentials via the SERCA and plasmalemmal Ca^{2+}ATPase pumps and mitochondrial buffering (*5* in Fig. 6).

It is not yet clear whether pacemaker potential generation arises from the summation of STDs from a single or a number or electrically-coupled PICs. Indeed, additional entrainment of the amplitude and frequency of STDs into a pacemaker potential may well occur as the initial STD generated in PICs that express I_{CaT} stimulates neighbouring PICs that only express I_{CaL} to activate the Ca^{2+} mobilization mechanisms discussed above. Also, it is also not yet clear whether Kit-positive PICs are indeed the pacemaker cell, PIC-specific reporter mouse strains that allow the creation of genetically encoded Ca^{2+} indicator models and a complete transcriptome comparison of the cells within the stroma will be required before the unequivocal identification of the prostate pacemaker cell.

Pacemaker potentials, once generated, appear to propagate passively into neighbouring stromal SMCs via connexion 43 gap junctions as depolarizing transients, which, if sufficiently large, trigger the opening of SMC LVDCCs and the firing of a number of regenerative action potentials (the slow wave) to initiate excitation-contraction coupling (*6* in Fig. 6). The repolarizing phase of the action potentials and the refractory period between slow waves are regulated by voltage activation of I_{Kto} channels, as well the activation of BK channels involving the process of CICR from SMC RyR stores (*7* in Fig. 6) (39).

Nerve evoked modulation of slow waves

The prostate is richly innervated with sympathetic nerves as well as parasympathetic and sensory nerves (11). α1-adrencoeptor blockade of the prostatic contractions evoked upon electrical field stimulation is not complete so that there appears to be a species dependent release of other co-transmitters from the sympathetic nerves themselves or neighbouring parasympathetic and sensory nerves. In the guinea-pig prostate, sponta-

neous slow waves and presumably their pacemaker drive are little affected by blockers of nerve conduction (tetrodotoxin) or sensory (capsaicin), sympathetic (guanethidine, prazosin) or parasympathetic (atropine) neurotransmission (5). However, slow wave firing and their associated contractions are initiated (18) or accelerated by autonomic agents (5, 11, 35).

Electrical field stimulation consisting of a single pulse readily evokes a single excitatory junction potential (EJP) that does not trigger stromal contraction, however, repetitive nerve stimulation causes a summation of these EJPs so that they trigger a slow wave with its superimposed action potential discharge and stromal contraction (40). EJPs and the nerve-evoked contractions are inhibited by guanethidine and after P2X receptor desensitization with α,β-methyleneATP or P2X-receptor blockade with PPADS. P2X1 immuno-staining is also restricted to the smooth muscle bundles, while blockade of adenosine A_2 receptors or α2-adrenoceptors enhances EJP amplitudes (40). In contrast, α1-adrenoceptor antagonists only reduce nerve-evoked contractions without affecting EJP amplitudes (19, 40). Interestingly, PICs in culture that co-locate α1-adrenoceptor and connexion 43 proteins readily respond to applied norepinephrine in a manner blocked by phentolamine and prazosin (12). However, it is yet not established whether PICs also respond to applied purines.

Together these data suggest it is likely that nerve-released purines acting on SMC P2X1 receptors is responsible for EJP generation and the acceleration of slow wave firing. It is not yet clear whether nerve-released noradrenaline or bath applied sympathetic agonists are acting on α1-adrenoceptors located exclusively on PICs, or more likely, on both on PICs and stromal SMCs. Prostatic hyperplasia has been associated with an increased density in the number of stromal α1-adrenoceptors (41). Results such as these has informed the search for prostate selective α1A-adrenoceptor antagonists, such as tamsulosin (42) to alleviate the dynamic component of benign prostatic hyperplasia.

Conclusions

Spontaneous Ca^{2+} signals in PICs lead to the generation of pacemaker electrical activity that drives the firing of spontaneous slow waves and the development of tone in the prostatic stroma. PICs may also act as intermediates during sympathetic neurotransmission selectively responding to nerve-released noradrenaline and maybe purines to enhance slow waves activity. Release from both RyRs and IP_3Rs is essential in PIC pacemaking and slow wave generation, although it is not clear which store acts as the initiator or the amplifier of this Ca^{2+} mobilization (43). Ca^{2+} influx through TVDCCs and the selective activation of CaCCs within a restricted sub-membrane space and signal amplification upon Ca^{2+} influx through LVDCCs may well be essential steps (the 'voltage sensor') (38) in inducing the release of stored Ca^{2+} and the synchronized activation of CaCCs to create a pacemaker potential. This dependence of PICs on LVDCC *and* TVDCC Ca^{2+} entry for the initiation of Ca^{2+} store release differs from interstitial cell pacemaking in the urethra where Ca^{2+} entry via the reversal flow through the Na^{+}: Ca^{2+} exchanger appears essential (43).

Conflict of Interest

The authors declare no conflicts of interest.

Abbreviations

AP	anterior prostate
BK channel	large conductance calcium-activated potassium channel
$[Ca^{2+}]_i$	intracellular concentration of Ca^{2+}
CaCC	Ca^{2+} activated Cl^- channel
CCCP	cyanide m-chlorphenyl hydrazine
Con	control
CPA	cyclopiazonic acid
CX43	connexion 43
CZ	central zone
FCCP	p-trifluoromethoxy carbonyl cyanide phenyl hydrazine
CGRP	calcitonin gene-related peptide
CICR	Ca^{2+} induced Ca^{2+} release
DIDS	4.4'-diisothiocyanostilbene-2,2' disulphonic acids
DP	dorsal prostate
ED	ejaculatory ducts
K_{ATP} channel	glibenclamide-sensitive ATP-dependent K^+ channel
I_{Ca}	Ca^{2+} current
I_{CaT}	TVDCC current
I_{CaL}	LVDCC current
ICC	interstitial cells of Cajal
ICC-IM	intramuscular ICC
I_{Kto}	transient K^+ current
IP_3	inositol trisphosphate
IP_3R	IP_3 receptor
LP	lateral prostate
LVDCC	L-type voltage-dependent Ca^{2+} channel
NFA	niflumic acid
Nif	nifedipine
PIC	prostate interstitial cell
PIP_2	phosphatidylinositol 4,5-bisphosphate
PLC	phospholipase C
PZ	peripheral zone
RyR	ryanodine receptor
SERCA	sacro-endoplasmic reticulum Ca^{2+}ATPase
SK channel	small conductance calcium-activated potassium channel
SNP	sodium nitroprusside
STD	spontaneous transient depolarization
SMC	smooth muscle cell
TEA	tetraethylammonium
TVDCC	T-type voltage-dependent Ca^{2+} channel
TZ	transitional zone
Ver	vernumontanum
VP	ventral prostate
2-APB	aminoethoxy-diphenylborate
4-AP	4-aminopyridine
9-AC	anthracene-9-carboxylic acid

References

1. Bhavsar A, Verma S. Anatomic imaging of the prostate. BioMed Res Int. 2014; 2014: 728539 [CrossRef]. [Medline]
2. Oliveira DS, Dzinic S, Bonfil AI, Saliganan AD, Sheng S, Bonfil RD. The mouse prostate: a basic anatomical and histological guideline. Bosn J Basic Med Sci. 2016; 16(1): 8–13. [Medline]
3. Berquin IM, Min Y, Wu R, Wu H, Chen YQ. Expression signature of the mouse prostate. J Biol Chem. 2005; 280(43): 36442–51. [Medline] [CrossRef]
4. Horsfall DJ, Mayne K, Ricciardelli C, Rao M, Skinner JM, Henderson DW, Marshall VR, Tilley WD. Age-related changes in guinea pig prostatic stroma. Lab Invest. 1994; 70(5): 753–63. [Medline]
5. Exintaris B, Klemm MF, Lang RJ. Spontaneous slow wave and contractile activity of the guinea pig prostate. J Urol. 2002; 168(1): 315–22. [Medline] [CrossRef]
6. Corradi LS, Jesus MM, Fochi RA, Vilamaior PS, Justulin LA Jr, Góes RM, Felisbino SL, Taboga SR. Structural and ultrastructural evidence for telocytes in prostate stroma. J Cell Mol Med. 2013; 17(3): 398–406. [Medline] [CrossRef]
7. Leong KG, Wang BE, Johnson L, Gao WQ. Generation of a prostate from a single adult stem cell. Nature. 2008; 456(7223): 804–8. [Medline] [CrossRef]
8. Van der Aa F, Roskams T, Blyweert W, De Ridder D. Interstitial cells in the human prostate: a new therapeutic target? Prostate. 2003; 56(4): 250–5. [Medline] [CrossRef]
9. Shafik A, Shafik I, el-Sibai O. Identification of c-kit-positive cells in the human prostate: the interstitial cells of Cajal. Arch Androl. 2005; 51(5): 345–51. [Medline] [CrossRef]
10. Kusljic S, Exintaris B. The effect of estrogen supplementation on cell proliferation and expression of c-kit positive cells in the rat prostate. Prostate. 2010; 70(14): 1555–62. [Medline] [CrossRef]
11. Exintaris B, Nguyen DTT, Dey A, Lang RJ. Spontaneous electrical activity in the prostate gland. Auton Neurosci. 2006; 126-127: 371–9. [Medline] [CrossRef]
12. Wang JP, Ding GF, Wang QZ. Interstitial cells of Cajal mediate excitatory sympathetic neurotransmission in guinea pig prostate. Cell Tissue Res. 2013; 352(3): 479–86. [Medline] [CrossRef]
13. Shigemasa Y, Lam M, Mitsui R, Hashitani H. Voltage dependence of slow wave frequency in the guinea pig prostate. J Urol. 2014; 192(4): 1286–92. [Medline] [CrossRef]
14. Imura M, Kojima Y, Kubota Y, Hamakawa T, Yasui T, Sasaki S, Hayashi Y, Kohri K. Regulation of cell proliferation through a KIT-mediated mechanism in benign prostatic hyperplasia. Prostate. 2012; 72(14): 1506–13. [Medline] [CrossRef]
15. Guo JH, Zhou J, Zhao Y, Liu PY, Yao HJ, Da J, Zhang M, Zhou Z, Chen Q, Peng YB, Wang Z. Normal peripheral prostate stromal cells stimulate prostate cancer development: roles of c-kit signal. Am J Transl Res. 2015; 7(3): 502–12. [Medline]
16. Canda AE, Dogan H, Kandemir O, Atmaca AF, Akbulut Z, Balbay MD. Does diabetes affect the distribution and number of interstitial cells and neuronal tissue in the ureter, bladder, prostate, and urethra of humans? Cent European J Urol. 2014; 67(4): 366–74. [Medline]
17. Aumüller G, Habenicht UF, el Etreby MF. Pharmacologically induced ultrastructural and immunohistochemical changes in the prostate of the castrated dog. Prostate. 1987; 11(3): 211–8. [Medline] [CrossRef]
18. Ohkawa H. Sympathetic neuromuscular transmission in the smooth muscle of guinea-pig prostate gland. Int J Fertil. 1983; 28(2): 68–77. [Medline]
19. Seki N, Suzuki H. Electrical and mechanical activity of rabbit prostate smooth muscles in response to nerve stimulation. J Physiol. 1989; 419: 651–63. [Medline] [CrossRef]
20. Hayase M, Hashitani H, Yanai Y, Kubota Y, Kojima Y, Sasaki S, Suzuki H, Kohri K. Mechanisms of

human prostate smooth muscle spontaneous contraction. J Urol. 2008; 179(4): 454. [CrossRef]

21. Exintaris B, Lee S, Chakrabarty B, Wittmer B, Ellem S, Lawrentschuk N, Frydenberg M, Papargiris M, Wilkinson S, Ricke W, Middendorff R, Risbridger G. Variability in the Spontaneous Contractility Profile of the Human Prostate Gland: Implications for a Personalized Treatment Approach to Better Manage Bph. Neurourol Urodyn. 2016; 35: S178–9.
22. Lang RJ, Nguyen DTT, Matsuyama H, Takewaki T, Exintaris B. Characterization of spontaneous depolarizations in smooth muscle cells of the Guinea pig prostate. J Urol. 2006; 175(1): 370–80. [Medline] [CrossRef]
23. Nguyen DTT, Lang RJ, Exintaris B. K^+ channel modulation of slow wave activity in the guinea-pig prostate. Br J Pharmacol. 2007; 151(6): 828–36. [Medline] [CrossRef]
24. Exintaris B, Nguyen DT, Lam M, Lang RJ. Inositol trisphosphate-dependent Ca stores and mitochondria modulate slow wave activity arising from the smooth muscle cells of the guinea pig prostate gland. Br J Pharmacol. 2009; 156(7): 1098–106. [Medline] [CrossRef]
25. Lam M, Shigemasa Y, Exintaris B, Lang RJ, Hashitani H. Spontaneous Ca^{2+} signaling of interstitial cells in the guinea pig prostate. J Urol. 2011; 186(6): 2478–86. [Medline] [CrossRef]
26. Dey A, Kusljic S, Lang RJ, Exintaris B. Role of connexin 43 in the maintenance of spontaneous activity in the guinea pig prostate gland. Br J Pharmacol. 2010; 161(8): 1692–707. [Medline] [CrossRef]
27. Dey A, Nguyen DT, Lang RJ, Exintaris B. Spontaneous electrical waveforms in aging guinea pig prostates. J Urol. 2009; 181(6): 2797–805. [Medline] [CrossRef]
28. Hashitani H, Fukuta H, Takano H, Klemm MF, Suzuki H. Origin and propagation of spontaneous excitation in smooth muscle of the guinea-pig urinary bladder. J Physiol. 2001; 530(Pt 2): 273–86. [Medline] [CrossRef]
29. Eckert RE, Schreier U, Drescher P, Madsen PO, Derouet H, Becht E, Steffens J, Ziegler M. Regulation of prostatic smooth muscle contractility by intracellular second messengers: implications for the conservative treatment of benign prostatic hyperplasia. Urol Int. 1995; 54(1): 6–21. [Medline] [CrossRef]
30. Sui GP, Wu C, Fry CH. Ca^{2+} currents in smooth muscle cells isolated from human prostate. Prostate. 2004; 59(3): 275–81. [Medline] [CrossRef]
31. Lang RJ, Mulholland E, Exintaris B. Characterization of the ion channel currents in single myocytes of the guinea pig prostate. J Urol. 2004; 172(3): 1179–87. [Medline] [CrossRef]
32. Lang RJ, Tonta MA, Takano H, Hashitani H. Voltage-operated Ca^{2+} currents and Ca^{2+} -activated Cl^- currents in single interstitial cells of the guinea-pig prostate. BJU Int. 2014; 114(3): 436–46. [Medline]
33. Oh SJ, Kim KM, Chung YS, Hong EK, Shin SY, Kim SJ. Ion-channel currents of smooth muscle cells isolated from the prostate of guinea-pig. BJU Int. 2003; 92(9): 1022–30. [Medline] [CrossRef]
34. Kito Y. The functional role of intramuscular interstitial cells of Cajal in the stomach. J Smooth Muscle Res. 2011; 47(2): 47–53. [Medline] [CrossRef]
35. Nguyen DT, Lang RJ, Exintaris B. alpha(1)-adrenoceptor modulation of spontaneous electrical waveforms in the guinea-pig prostate. Eur J Pharmacol. 2009; 608(1-3): 62–70. [Medline] [CrossRef]
36. Hirst GD, Ward SM. Interstitial cells: involvement in rhythmicity and neural control of gut smooth muscle. J Physiol. 2003; 550(Pt 2): 337–46. [Medline] [CrossRef]
37. Lang RJ, Tonta MA, Zoltkowski BZ, Meeker WF, Wendt I, Parkington HC. Pyeloureteric peristalsis: role of atypical smooth muscle cells and interstitial cells of Cajal-like cells as pacemakers. J Physiol. 2006; 576(Pt 3): 695–705. [Medline] [CrossRef]
38. Berridge MJ. Smooth muscle cell calcium activation mechanisms. J Physiol. 2008; 586(21): 5047–61. [Medline] [CrossRef]
39. Burdyga T, Wray S. Action potential refractory period in ureter smooth muscle is set by Ca sparks and BK channels. Nature. 2005; 436(7050): 559–62. [Medline] [CrossRef]
40. Lam M, Mitsui R, Hashitani H. Electrical properties of purinergic transmission in smooth muscle of the

guinea-pig prostate. Auton Neurosci. 2016; 194: 8–16. [Medline] [CrossRef]

41. Yamada S, Ashizawa N, Ushijima H, Nakayama K, Hayashi E, Honda K. Alpha-1 adrenoceptors in human prostate: characterization and alteration in benign prostatic hypertrophy. J Pharmacol Exp Ther. 1987; 242(1): 326–30. [Medline]
42. Chakrabarty B, Dey A, Lam M, Ventura S, Exintaris B. Tamsulosin modulates, but does not abolish the spontaneous activity in the guinea pig prostate gland. Neurourol Urodyn. 2015; 34(5): 482–8. [Medline] [CrossRef]
43. Drumm BT, Large RJ, Hollywood MA, Thornbury KD, Baker SA, Harvey BJ, McHale NG, Sergeant GP. The role of Ca(2+) influx in spontaneous Ca(2+) wave propagation in interstitial cells of Cajal from the rabbit urethra. J Physiol. 2015; 593(15): 3333–50. [Medline] [CrossRef]
44. Hashitani H, Lang RJ. Functions of ICC-like cells in the urinary tract and male genital organs. J Cell Mol Med. 2010; 14(6A): 1199–211. [Medline] [CrossRef]